PROCEEDINGS A

rspa.royalsocietypublishing.org

Research

Article submitted to journal

Subject Areas:
Colloid Science, Polymer Chemistry, Condensed Matter Physics

Keywords:
Colloids, Light Scattering, X-ray Scattering, Transparent Dispersions

Author for correspondence:
Gregory N. Smith
e-mail: gregory.smith@nbi.ku.dk

Refractive index matched, nearly hard polymer colloids

Gregory N. Smith[1,*], Matthew J. Derry[1], James E. Hallett[2,†], Joseph R. Lovett[1], Oleksander O. Mykhaylyk[1], Thomas J. Neal[1], Sylvain Prévost[3,‡], and Steven P. Armes[1]

[1] Department of Chemistry, University of Sheffield, Brook Hill, Sheffield, South Yorkshire, S3 7HF, UK
[2] H. H. Wills Physics Laboratory, Tyndall Avenue, University of Bristol, Bristol, BS8 1FD, UK
[3] ESRF, The European Synchrotron, 71 Avenue des Martyrs, 38000 Grenoble, France

Refractive index matched particles serve as essential model systems for colloid scientists, providing *nearly* hard spheres to explore structure and dynamics. The PMMA latexes typically used are often refractive index matched by dispersing them in a binary solvent mixture, but this can lead to undesirable changes, such as particle charging or swelling. To avoid this shortcoming, we have synthesised refractive index matched colloids using polymerisation-induced self-assembly (PISA) rather than as polymer latexes. The crucial difference is that these diblock copolymer nanoparticles consist of a *single core-forming* polymer in a *single* non-ionisable solvent. The diblock copolymer chosen was poly(stearyl methacrylate)–poly(2,2,2-trifluoroethyl methacrylate) (PSMA–PTFEMA), which self-assembles to form PTFEMA core spheres in *n*-alkanes. By monitoring scattered light intensity, *n*-tetradecane was found to be the optimal solvent for matching the refractive index of such nanoparticles. As expected for PISA syntheses, the diameter of the colloids can be controlled by varying the PTFEMA degree of polymerisation. Concentrated dispersions were prepared, and the diffusion of the PSMA–PTFEMA nanoparticles as a function of volume fraction was measured. These diblock copolymer nanoparticles are a promising new system of transparent spheres for future colloidal studies.

THE ROYAL SOCIETY PUBLISHING

1. Introduction

Noninteracting hard sphere colloids are essential tools for experimentally studying interparticle interactions to compare to theory, and polymer colloids in nonaqueous solvents are one of the best model systems for these studies [1]. Perhaps the most significant early report of polymer colloids designed to be transparent, hard spheres came from Pusey and van Megen in 1986, who showed that poly(methyl methacrylate) (PMMA) latexes in a mixture of decalin and carbon disulfide were refractive index matched and formed colloidal crystals [2]. The refractive index difference can be related to the strength of dispersion or van der Waals attractions, and matching the refractive indices of the dispersed and continuous phases will minimise attraction at short separations [3]. There are other nanoparticles that have been studied as either effectively hard or refractive index matched colloids, such as sterically-stabilised PMMA in *cis*-decalin alone [4,5], silica in ethylene glycol [6], or poly-*N*-isopropylacrylamide (PNIPAM) in water [7–9], but on balance, PMMA colloids in a low polarity medium are considered to be the best system of experimental nearly hard sphere colloids [1]. Refractive index matching PMMA latexes has been achieved in the past using several approaches. One is by dispersing PMMA particles in a binary solvent mixture consisting of one high-refractive index solvent (such as a cycloalkylbromide, tetrachloroethylene, or carbon disulfide) and *cis*-decalin [1,2,10–17]. The other is by polymerising a low-refractive index comonomer, a fluorinated acrylate or methacrylate, along with MMA [18–31]. These methods require using either a multicomponent solvent mixture or a statistical copolymer core, meaning that much experimental work is required to identify the precise ratio required for refractive index matching. Additionally, dispersing the colloids in a binary solvent mixture, as is most commonly done, can either charge particles due to solvent autoionisation [12] or swell the particles due to solvent partitioning to the core [32]. Although popular, the binary solvent approach has some potential disadvantages that could result in making the particles unsuitable for use as hard spheres. The salt typically used to screen charges is saturated at a concentration that only reduces the Debye length to 100s of nm [1]. Using a salt with a higher solubility, though, can result in loss of colloidal stability at high salt concentrations [33]. Other solvents, such as carbon disulfide, chloroform and tetrachloroethylene, can swell the particles instead. [1,10] This results in particles with an unpredictable radius and a changing density, and consequently, a dispersion that is no longer refractive index matched. [1] Although it is possible to ameliorate these issues by adding salts or adjusting the amount of dense solvent until the system reaches a steady state, they make refractive index matched polymer colloids that consist of a single core-forming polymer in a single, non-ionisable solvent, which would not require such adjustments, highly desirable.

There are a myriad of reports in the literature of ways to prepare various spherical colloids consisting of, for example, silica (Stöber synthesis), poly(12-hydroxystearic acid)-stabilised PMMA, poly(vinylpyrrolidone)-stabilised polystyrene, and PNIPAM [8,9,34–37]. Sterically-stabilised PMMA latexes are probably the best model for experimental hard spheres [1], and we take these spheres as our inspiration to synthesise aliphatic polymer-stabilised poly(methacrylate) spheres in a low dielectric solvent. We are particularly interested in studying polymer colloids, because of the ease by which functional units can be introduced into the particles without significantly modifying their colloidal properties [38,39]. Previous reports of refractive index matched polymer colloids typically used dispersion polymerisation to prepare sterically-stabilised *latexes*. In this study, we report using a different method to prepare well-defined diblock copolymer nanoparticles. Rather than polymer latexes, which tend to be well-defined for particles with diameters of 100s of nm to several μm, we have synthesised well-defined diblock copolymers that form *polymer micelles*, which tend to be well-defined even under 100 nm. Particles of a smaller size will be an interesting addition to the available systems of refractive index matched, nearly hard sphere colloids. This small size means that the particles will sediment much more slowly, reducing the necessity to density match them as well, and that they will extend the

range of sizes available an order of magnitude smaller than before. We used polymerisation-induced self-assembly (PISA) as the method to make these spherical nanoparticles. It has been developed for the rational synthesis of sterically-stabilised polymer colloids. Using reversible addition–fragmentation chain-transfer (RAFT) polymerisation, a soluble macromolecular chain-transfer agent (macro-CTA) is chain-extended using a suitable second monomer to form an insoluble polymer, resulting in *in situ* self-assembly [40]. This procedure does involve two steps: the synthesis and purification of the macro-CTA and its chain extension to produce a diblock copolymer nanoparticle. It is possible for some formulations to synthesise the particles in a sequential one-pot reaction, and this has been demonstrated for several systems in non-polar solvents [41,42]. The rational production of particles with a predictable size based on the core degree of polymerisation (DP) and the purity of the final particles mean that even this two-step synthesis is worthwhile.

Using PISA, it has been possible to synthesise diblock copolymer nano-objects in water [43], lower alcohols [44,45], and non-polar solvents [44]. Various polymers have been used to form the core-forming blocks of PISA-synthesised nano-objects in non-polar solvents, including poly(methyl acrylate) [46–48], poly(benzyl methacrylate) [41,49–56], poly(3-phenylpropyl methacrylate) [57–59], poly(benzyl acrylate) [42], poly(*n*-2-(methacryloyloxy)ethyl pyrrolidone) [60], poly(phenyl acrylate) [61], and poly(2,2,2-trifluoroethyl methacrylate) [62].

In this paper, polymer colloids were synthesised using poly(2,2,2-trifluoroethyl methacrylate) (PTFEMA) as a low-refractive index core-forming block, which should enable the formation of almost perfectly refractive index matched nanoparticles in non-polar solvents. A nearly transparent dispersion is a prerequisite to obtaining a system of nearly hard spheres. Regardless of the interparticle interactions, the dispersion attraction is minimised in a refractive index matched systems [3]. Indeed, PTFEMA has been shown to be a feasible core-forming block for visible light spectroscopy in non-polar solvents, due to its near refractive index matching [62]. This optical transparency afforded by refractive-index matching has enabled PISA-synthesised PTFEMA-based nano-objects in other solvents as well to form highly transparent Pickering emulsions and monitor the character of the polymerisation [63,64], but the behaviour of the colloids themselves has not previously been considered. As the particles are synthesised in non-polar solvents, poly(stearyl methacrylate) (PSMA) was selected as a steric stabiliser, due to its established ability to stabilise copolymer nano-objects in such media [52,53,55,57–60]. The PISA synthesis route is shown in Scheme 1. Unlike the previous reports of partly-fluorinated particles by PISA [63,64], we focus on the synthesis of nano-objects directly in *n*-alkane solvents to identify the single solvent that best matches the refractive index of these PSMA–PTFEMA nano-objects. These dispersions should, therefore, meet the aim of obtaining colloids of a single polymer core in a single solvent while avoiding the problems of particle charging and particle swelling inherent in using refractive index matched PMMA latexes. The characterisation of these polymer colloids suggests ways that these highly transparent dispersions can be employed by colloid scientists, and we anticipate that they will become a useful model system in due course.

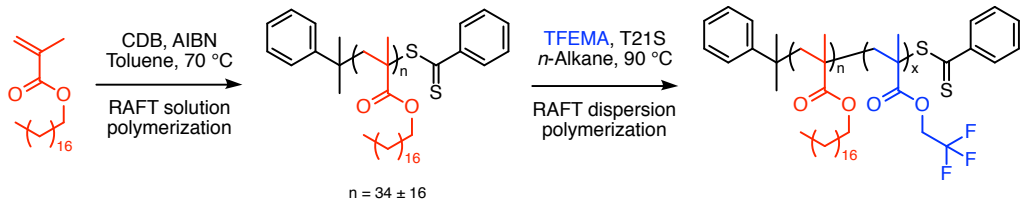

Scheme 1. Synthesis of a poly(stearyl methacrylate) (PSMA) macro-CTA via RAFT solution polymerisation in toluene at 70 °C, followed by RAFT dispersion polymerisation of 2,2,2-trifluoroethyl methacrylate (TFEMA) in an *n*-alkane at 90 °C to give a PSMA–PTFEMA diblock copolymer.

2. Experimental

(a) Materials

Stearyl methacrylate (SMA, technical grade), and 2,2,2-trifluoroethyl methacrylate (TFEMA, 96%) monomers were purchased from Sigma–Aldrich (UK). TFEMA monomer was passed over a basic alumina column to remove inhibitor prior to use. 2,2′-Azobisisobutyronitrile (AIBN) initiator was purchased from Molekula (UK), and *tert*-butyl peroxy-2-ethylhexanoate (T21S) initiator was a gift from AkzoNobel (The Netherlands). Cumyl diothiobenzoate (CDB, 99%) RAFT agent was purchased from Sigma–Aldrich (UK) and used as supplied. Solvents for synthesis and purification (toluene, ethanol) were purchased from either VWR, Sigma–Aldrich, or Fisher (UK) and were used as supplied. Deuterated solvents were obtained from either Cambridge Isotope Laboratories (USA) (dichloromethane-d_2) or Sigma–Aldrich (UK) (chloroform-d_3). The four *n*-alkanes used were either obtained from Sigma–Aldrich (*n*-dodecane, $\geq 99\%$) or Alfa Aesar (*n*-decane, 99%; *n*-tetradecane, 99%; and *n*-hexadecane, 99%) and were used as provided.

(i) Poly(stearyl methacrylate) macromolecular chain transfer agent (macro-CTA)

SMA (20.02 g, 59.1 mmol), CDB (0.58 g, 2.1 mmol), and AIBN (0.0699 g, 0.43 mmol; CDB/AIBN molar ratio = 5.0) were dissolved in toluene. The solution was purged with nitrogen and then heated at 70 °C for 10 h. The crude PSMA was purified by precipitation into ethanol. The polymerisation was taken to 75% conversion as judged by ^{1}H NMR in CD_2Cl_2, and the purified polymer was characterised using gel permeation chromatography (GPC) in THF (PMMA standards) to determine the molar mass ($M_n = 13,200$ g mol^{-1} and $M_w = 15,000$ g mol^{-1}) and dispersity ($Đ_M = M_w/M_n = 1.14$) as well as by ^{1}H NMR in CD_2Cl_2 to determine the DP by comparing integrated CDB aromatic protons at 7.1–8.1 ppm with the two PSMA oxymethylene protons at 3.8–4.0 ppm (PSMA DP = 34). The standard deviation of the DP (± 16) was calculated using Harrisson's method [65].

(ii) Poly(stearyl methacrylate)–poly(2,2,2-trifluoroethyl methacrylate) diblock copolymers

Poly(stearyl methacrylate)–poly(2,2,2-trifluoroethyl methacrylate) ($PSMA_{34}$–$PTFEMA_x$, where x is the PTFEMA DP) diblock copolymers were synthesised using a $PSMA_{34}$ macro-CTAs using a modified approach based on previous work with benzyl methacrylate [52], see Scheme 1. The macro-CTA and initiator were dissolved in the specified *n*-alkane at a total concentration of 20 wt. %. The $PSMA_{34}$ macro-CTA was added as a solid, and the T21S initiator was added as a 10 wt. % solution in *n*-dodecane (TS1s/macro-CTA molar ratio = 3). The initiator was dissolved in *n*-dodecane regardless of the alkane solvent used, but the amount of *n*-dodecane relative to the total amount of *n*-alkane solvent was negligible. This solution was degassed using nitrogen for 30 min. TFEMA monomer was degassed using nitrogen for 30 min separately due to its volatility and added to the macro-CTA and initiator solution volumetrically. (The mass added was recorded.) The reaction solution was then degassed for a further 10 min, heated to 90 °C, and allowed to proceed for at least 18 h. All diblock copolymers were analysed using ^{1}H NMR to calculate the final DP and ^{19}F NMR (both in $CDCl_3$) to calculate the monomer-to-polymer conversion. They were also analysed using GPC with THF eluent (PMMA standards) with refractive index detection, so the GPC-determined molar mass distributions are artificially broad. This is due to the refractive index detector being more sensitive to the PSMA block than the PTFEMA block, because the refractive index difference is greater between PSMA and THF than PTFEMA and THF [63]. Characterisation of the polymers is given in the Supporting Information (Sections S1–S3).

The as-synthesised dispersions (20 wt. %) were used directly for static light scattering. Dispersions were diluted for dynamic light scattering, small-angle X-ray scattering, and transmission electron microscopy analysis. For the dynamic light scattering measurements on concentrated dispersions, a 20 wt. % dispersion was centrifuged at 10k rpm for 3 h and a

measured mass of solvent removed to obtain a high concentration stock. This was then diluted to give dispersions of a desired volume fraction (ϕ). Volume fractions were obtained gravimetrically (the "measuring mass and density" method described by Poon *et al*. [17]). The initial known masses of particles (m_p) and solvent (m_s) as well as the new solvent (of the same type) added or removed (m_a) were converted to a volumes using the mass densities (ρ_m, with the appropriate subscript for the species) to calculate the volume fraction of the dispersion that was occupied by the polymer spheres (ϕ).

$$\phi = \frac{m_p}{\rho_{m,p}} + \frac{m_s}{\rho_{m,s}} \pm \frac{m_a}{\rho_{m,s}} \tag{2.1}$$

(b) Methods

(i) Dynamic and static light scattering (DLS and SLS)

DLS and SLS measurements were performed to determine either the diffusion coefficient (DLS) or the amount of scattered light (SLS) using a Malvern Zetasizer Nano ZS (Malvern Instruments, UK). The wavelength of the radiation was $\lambda = 632.8$ nm, and the scattering angle was 173°. For a light scattering measurement, the modulus of the momentum transfer vector $\vec{Q}$ is defined in 2.2, where θ is half the scattering angle and n is the refractive index.

$$Q = \frac{4\pi n \sin\theta}{\lambda} \tag{2.2}$$

Q has the value 0.0028 Å^{-1} for these values. DLS measurements were performed on diluted dispersions (~ 1 vol. %), and SLS measurements were performed on as-synthesised dispersions. Optical glass cuvettes with a path length of 10 mm were used to load the dispersions. For all measurements, approximately 10 runs of 10 s duration were performed per measurement. (The exact number was selected by the instrument software.) Different numbers of measurements were used for the specific experiments: three (DLS measurements on dilute dispersions), 15 (DLS measurements on concentrated dispersions), and one (SLS).

(ii) Small-angle X-ray scattering (SAXS)

SAXS measurements were performed using two instruments: an in-house Bruker AXS Nanostar (The University of Sheffield, UK) and the synchrotron beamline ID02 at the ESRF (Grenoble, France). The modulus of momentum transfer vector $\vec{Q}$ is defined in Equation 2.3, where θ is half the scattering angle and λ is the wavelength of the X-ray radiation.

$$Q = \frac{4\pi \sin\theta}{\lambda} \tag{2.3}$$

The Bruker AXS Nanostar instrument (Cu K-α radiation and 2D HiSTAR multiwire gas detector), modified with a microfocus X-ray tube (GeniX3D, Xenocs, France) and two sets of motorised scatterless slits for the beam collimation, was set to a sample-detector distance $L = 1.46$ m. SAXS patterns were recorded over a Q range of 0.008 Å$^{-1} < Q < 0.15$ Å^{-1}. Glass capillaries of 2.0 mm diameter were used as a sample holder, and an exposure time of 600 s was used for each sample data collection. Two-dimensional SAXS data were reduced to one-dimensional SAXS curves using Nika macros for Igor Pro [66].

The beamline ID02 used monochromatic X-ray radiation ($\lambda = 0.995$ Å) and a Rayonix MX-170HS CCD detector. A sample-detector distance $L = 6$ m was set to obtain an effective Q-range after data reduction of 0.003 Å$^{-1} < Q < 0.09$ Å^{-1}. For $PSMA_{34}$–$PTFEMA_{568}$ nanoparticles, an additional sample-detector distance of $L = 30$ m was used to obtain a minimum Q of 3×10^{-4} Å^{-1}, and data were fit from $Q > 0.001$ Å^{-1}, due to issues with background subtraction at lower-Q. Glass capillaries of 2 mm diameter were used as a sample holder, and exposure times of 0.02–1 s were used for the SAXS data collection. Scattering data were automatically reduced using the standard workflow at the beamline [67]. Water was used as a standard for the absolute intensity calibration.

All one-dimensional SAXS data collected by different instruments were processed (normalisation and background subtraction) using Irena SAS macros for Igor Pro [68]. Data were fit as described in the text using bespoke models implemented for Irena SAS macros for Igor Pro [68].

(iii) Transmission electron microscopy (TEM)

TEM imaging was performed on FEI Tecnai Spirit microscope fitted with a Gatan 1kMS600CW CCD camera operating at 80 kV. Copper/palladium TEM grids (Agar Scientific, UK) were surface-coated in-house to yield a thin film of amorphous carbon. The copolymer dispersion was diluted in *n*-dodecane at ambient temperature to produce a 0.1 wt. % dispersion. 10 μL of this dispersion was deposited onto the surface of the on carbon-coated copper TEM grid. As the core-forming PTFEMA is semi-fluorinated, no stain was required to obtain contrast with the carbon-coated grid.

3. Results and Discussion

PSMA–PTFEMA diblock copolymer micelles were synthesised directly in the *n*-alkane of interest, as shown in Scheme 1, and were studied either directly as concentrated dispersions or after dilution by the *n*-alkane used for synthesis, depending on the requirements of the technique. The first task was to assess the *n*-alkane solvent that afforded the most transparent dispersions. After establishing the optimal *n*-alkane solvent, the polymer nano-objects were studied using various techniques. The nanoparticles have a high *X-ray* photon contrast with the solvent, due to the large difference in electron density, but a low *visible light* photon contrast, due to a small difference in the refractive index. These make them amenable to analysis by light scattering and X-ray scattering.

(a) Refractive index matching

The transparency of $PSMA_{34}$–$PTFEMA_x$ nanoparticle dispersions was used as a method of determining how well refractive matched the particles are to the solvents. In general, colloidal dispersions are turbid from the scattering of light. For otherwise equivalent particles, the intensity increases with increasing difference in refractive index between solute and solvent [69]. Transparent dispersions, therefore, will be obtained when the refractive index difference is minimised. Static light scattering was used to record the intensity of scattered light at a fixed wavelength and detector angle ($\lambda = 632.8$ nm and scattering angle of 173°) and, therefore, assess the amount of light scattered. A quantification of the turbidity of a series of diblock copolymers with a common composition ($PSMA_{34}$–$PTFEMA_{500}$) synthesised directly in four different *n*-alkanes at a concentration of 20 wt. % is shown in Figure 1(a). The *n*-alkanes (*n*-decane, *n*-dodecane, *n*-tetradecane, and *n*-hexadecane) were chosen as they had slightly different refractive indices that spanned the refractive index of PTFEMA homopolymer, known from the literature. (Refractive indices are shown in Table 1.)

Additionally, the particle size was determined using SAXS on dilute dispersions of $PSMA_{34}$–$PTFEMA_{500}$ in the *n*-alkane chosen for synthesis, shown in Figure 1(b). These measurements show that the colloids are approximately the same size and, therefore, a like-for-like comparison between the colloids in different solvents is justified. This is important as static light scattering intensity will depend on angle if the size changes. The SAXS model used to fit the data and the best fit parameters are shown in the Supporting Information (Sections S4 and S5). The $PSMA_{34}$–$PTFEMA_{500}$ spheres synthesised in *n*-decane do appear to be smaller than those synthesised in the other *n*-alkanes, but as this solvent is clearly the worst for refractive index matching the particles (Figure 1(a)), the size difference does not merit consideration. For the other particles in the other solvents, *n*-tetradecane is the best solvent for producing transparent dispersions

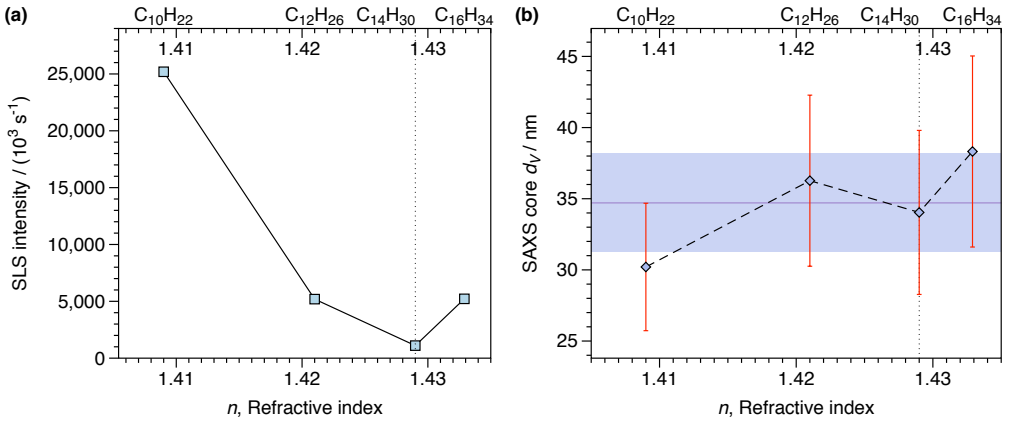

Figure 1. The (a) turbidity and (b) diameter of $PSMA_{34}$–$PTFEMA_{500}$ diblock copolymer micelles synthesised in four different *n*-alkanes (*n*-decane, $C_{10}H_{22}$; *n*-dodecane, $C_{12}H_{26}$; *n*-tetradecane, $C_{14}H_{30}$; and *n*-hexadecane, $C_{16}H_{34}$). Refractive indices are shown in Table 1. By SLS (intensity of scattered light from a static light scattering measurement), *n*-tetradecane is the best solvent for refractive index matching the particles. Particle sizes were determined by SAXS (volume-weighted core diameter, d_V) and are essentially unchanged, indicating that the solvent does not strongly impact the self-assembly. Error bars show one standard deviation of the Gaussian distribution in core diameter, and the shaded region shows one standard deviation of the mean diameter for all particles.

Table 1. Refractive index (n) of materials solvents and solutes.

	Refractive index, n
n-Decane	1.409
n-Dodecane	1.421
n-Tetradecane	1.429
n-Hexadecane	1.433
PSMA	1.501
PTFEMA	1.416

Values for *n*-alkanes from CRC Handbook [70], for PSMA from Tamada *et al*. [71], and for PTFEMA from Yoshioka *et al*. [72].

of $PSMA_{34}$–$PTFEMA_{500}$ spheres. This, therefore, is the solvent studied for preparing refractive index matched dispersions.

Determining the optimal solvent for refractive index matching experimentally rather than relying on *a priori* analysis of the material properties (Table 1) is essential. *n*-Tetradecane does appear to be the best solvent for matching $PSMA_{34}$–$PTFEMA_{500}$ spheres, but it is not the solvent that has a refractive index nearest to that of PTFEMA homopolymer (Table 1). This is because these nanoparticles consist of diblock copolymers, and therefore, the effective refractive index is a composite of that of PSMA and PTFEMA homopolymers. A simple mixing rule was used to determine the refractive index of the composite particle (n_p), where n_i is the refractive index of the i-th component and ϕ_i is its volume fraction.

$$n_p = \sum_i n_i \phi_i \tag{3.1}$$

Despite the simplicity of Equation 3.1, the relatively small particle size and the fact that they are nearly refractive index matched makes it appropriate [73]. The relative particle diameter ($(2\pi a)/\lambda$,

where a is the radius) is low, and the relative refractive index ($m_r = n_p/n_m$, where n_m is the refractive index of the medium) is ~ 1. Under these conditions, the empirical mixing rule is valid [73]. For the calculation, the refractive index of the particle was set equal to that of *n*-tetradecane. For each nanoparticle, using the literature values of the polymer refractive indices shown in Table 1, this gives a volume fraction of each polymer within the nanoparticle of 0.85 for PTFEMA and of 0.15 for PSMA, which is comparable to that expected based on the block volumes alone (0.91 for PTFEMA and 0.09 for PSMA).

This demonstrates that the internal structure of the colloid needs to be considered and that experimental verification needs to be performed to assess the optimal refractive index match. The system studied here, PSMA–PTFEMA diblock copolymer spheres in *n*-tetradecane, is the best solvent for refractive index matching these specific diblock copolymer nanoparticles. However, it is feasible that for some compositions, *n*-dodecane or *n*-hexadecane, for example, are the best alkane solvent for refractive index matching particles. For example, a recent report showed that *n*-dodecane was best solvent for refractive index matching $PSMA_{32}$–$PTFEMA_{490}$ diblock copolymer nanoparticles, which are similar in block composition to those studied here albeit with a different RAFT agent and a much larger particle size [62]. The transparency of these nanoparticle dispersions, therefore, can vary as a function of temperature, wavelength of radiation, or particle size, for instance. It is worthwhile verifying experimentally the quality of the refractive index matching between nanoparticle and solvent, but it is obvious that PSMA–PTFEMA colloids in *n*-alkanes are a very promising general motif for producing transparent colloidal dispersions.

(b) PSMA–PTFEMA diblock copolymer nano-objects

Having established that *n*-tetradecane is the best solvent for refractive index matching $PSMA_{34}$–$PTFEMA_{500}$, a series of $PSMA_{34}$–$PTFEMA_x$ nano-objects were synthesised with a range of PTFEMA DPs spanning an order of magnitude from ~ 100 to ~ 1000. DLS and SAXS measurements were performed on dilute dispersions of $PSMA_{34}$–$PTFMEA_x$ spheres in *n*-tetradecane to determine the diameters of the spheres as a function of DP. These data are shown in Figure 2(a) along with fitted SAXS data in Figure 2(b).

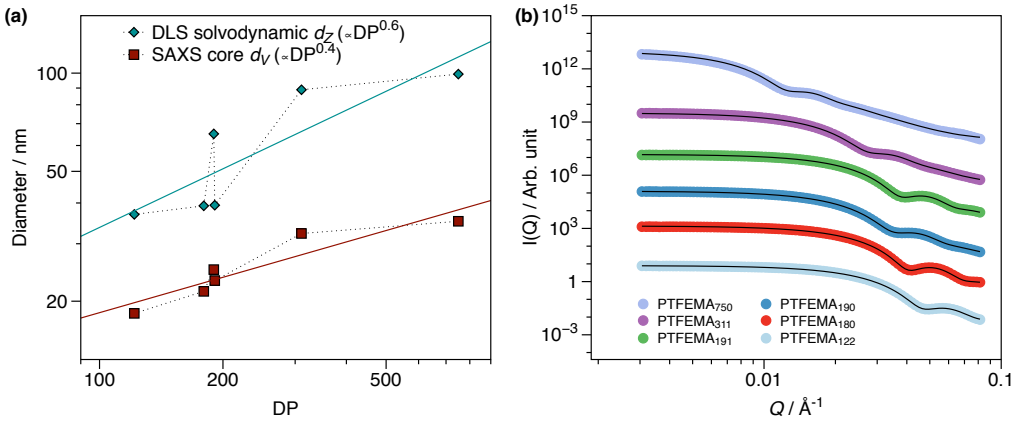

Figure 2. The (a) diameters of $PSMA_{34}$–$PTFEMA_x$ colloids in *n*-tetradecane and (b) SAXS data of the dilute (1 wt. %) dispersions. Diameters were measured using DLS (Z-average diameter, d_Z) and SAXS (volume-weighted PTFEMA core diameter, d_V). The diameters measured using both techniques increase as a power law function of PTFEMA DP shown. The polymer micelles form well-defined spheres with a rationally increasing diameter as shown in the fit SAXS data. The data fitting procedure is discussed in the text.

The diameters of the nanoparticles were determined using two different techniques. DLS measurements were performed on dilute dispersions (~ 1 wt. %), and the Z-average diameter of the particles are shown in Figure 2(a). The data are somewhat noisy, but this is because the dispersions are nearly transparent, so relatively little light is scattered. It is possible that impurities in the system that are not refractive index matched may contribute to the raw DLS data, and therefore, a technique with higher contrast is desirable. SAXS measurements were also performed on dilute dispersions with a concentration of ~ 1 wt % (volume distribution, d_V), and these data are much less noisy, because of the large electron density difference between PSMA–PTFEMA and n-tetradecane. The particles give well-defined SAXS (Figure 2(b)) curves that can be fit well by the appropriate copolymer micelle models, discussed in Supporting Information Section S4. The mean diameters increase as a power law of the PTFEMA DP ($d \propto \mathrm{DP}^{\alpha}$) with the power law exponent α relating to the degree of segregation of the phase separated polymer chains (α should range between 0.5 and 1), as has been shown for similar poly(stearyl methacrylate)–poly(benzyl methacrylate) nano-objects in non-polar solvents [52,55]. The fit values of α are very similar for the two sizing techniques: α of 0.6 for DLS d_Z and α of 0.4 for SAXS d_V. Differences in the α from different techniques for otherwise identical nanoparticles are known in the literature [55], and this is due to the different weighting and sensitivity of different techniques. Regardless, that the particle diameters increase as a power law of PTFEMA DP shows that spheres are the dominant morphology.

While spheres are the *dominant* morphology, a careful analysis of the scattering demonstrates that they are not the *exclusive* morphology. Indeed, PISA syntheses are known to give a wide range of morphologies other than spheres. Spheres, worms, and vesicles are typically obtained morphologies, but more exotic nanostructures such as lamellae, framboidal vesicles, oligolamellar vesicles, jellyfish, and yolk/shell particles have also been reported [40]. The raw SAXS curves (Figure 2(b)) are qualitatively consistent with only spherical nanoparticles: the scattering intensity at low-Q (the Guinier region) is proportional to Q^0 rather than Q^{-1} or Q^{-2}, as might be expected for a non-spherical species [74]. However, microscopy and scattering data of a dispersion of PSMA_{34}–PTFEMA_{568} diblock nanoparticles shows that there are a minor population of non-spherical nano-objects present. The TEM micrograph (inset in Figure 3) shows that the majority of nano-objects are spherical, but there is also a small population of dimers present. This is likely because either the PSMA DP is too low or the copolymer concentration is too high to "trap" spheres as the dominant morphology. Spherical polymer micelles are known to be the first step to form *in situ* even for higher order morphologies [75]. The SAXS data shown in Figure 3 support this observation; the best fit is achieved by accounting for a small population of dimers. The qualitative SAXS data make it possible to determine the relative fraction in each population (using the scale factor, which is proportional to the volume fraction of each population [74]). The models used to fit the SAXS data are discussed in Section S4 in the Supporting Information [52,76–80]. The spherical nanoparticle population were modelled using a well-known model, and the scattering from the dimers calculated using the spheres method and placing two spheres touching in close proximity. From the fitted scale factors, the sphere population occupies 94% of the volume and 97% of the number of nanoparticles in this dispersion. Eliminating the dimer population, perhaps by increasing the PSMA DP or decreasing the concentration of the stock dispersion, would be desirable for future studies.

(c) Characterisation of PSMA–PTFEMA nano-objects

Having established the rational synthesis of PSMA–PTFEMA nano-objects in n-tetradecane by PISA, a dispersion of PSMA_{34}–PTFEMA_{568} nanoparticles was synthesised on a larger scale (~ 50 g) to enable concentrated dispersions to be prepared. An advantage of these effectively transparent spheres is that they can be studied using multiple forms of scattering. The small refractive index difference (Table 1) means that the dispersions are highly transparent even up to very high volume fractions ($\phi \lesssim 0.5$). An image of the concentrated dispersions (in polyamide cells with a path length of 2 mm) is shown in Figure 4. Even up to $\phi = 0.54$, the dispersions

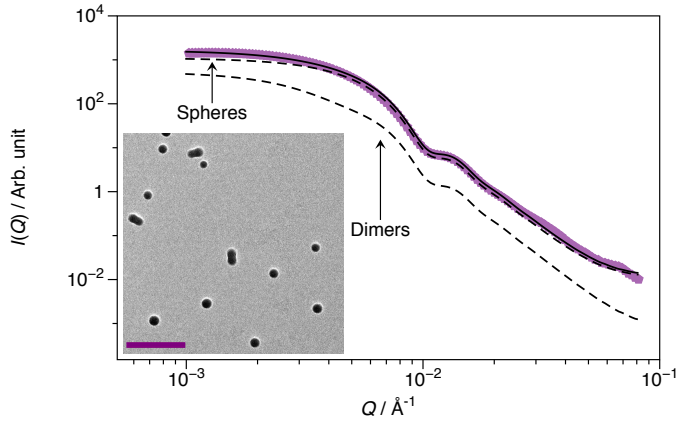

Figure 3. SAXS data and TEM micrograph (inset) of $PSMA_{34}$–$PTFEMA_{568}$ diblock copolymer nanoparticles in *n*-tetradecane. Spherical are the dominant morphology, but there is a minor population of copolymer micelle dimers present. The scale bar in the TEM micrograph is 500 nm.

are essentially transparent; only having a slight pink colour due to the dithiobenzoate RAFT agent [81]. On the other hand, the large electron density contrast means that the X-ray scattering length density is high (Table S9 in Supporting Information) and, therefore, the dispersions are well suited to analysis by X-ray scattering, as can be seen in Figures 2 and 3.

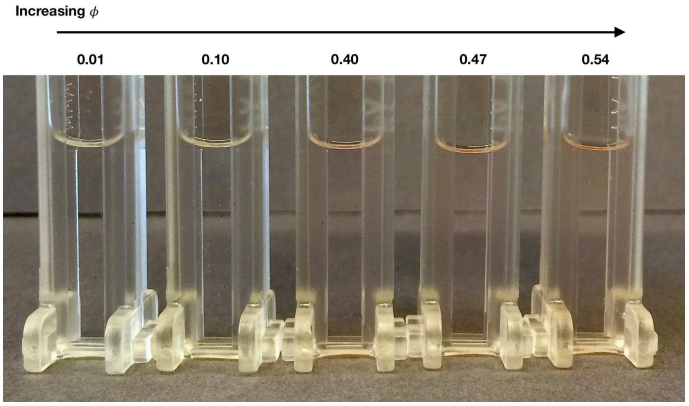

Figure 4. Digital photograph of concentrated dispersions of $PSMA_{34}$–$PTFEMA_{568}$ nanoparticles in *n*-tetradecane for $0.01 \leq \phi \leq 0.54$. These dispersions are highly transparent at all concentrations.

The bulk properties of concentrated dispersions can be strongly dependent on ϕ, therefore the compatibility of this system with various analytical techniques over a range of volume fractions is very beneficial. Typically, for hard spheres, the most commonly investigated bulk properties are the viscosity, diffusivity and the structure factor [17]. In this study, we prioritised the diffusivity and characterised the effect of increasing the volume fraction on the diffusion of the nanoparticles in the form of concentrated dispersions using DLS.

DLS is commonly used to determine solvodynamic particle diameters through the Stokes–Einstein equation, which relates the diffusion coefficient (D) to the solvodynamic radius (r) and

the thermal energy (k_BT) [82,83].

$$D = \frac{k_BT}{6\pi\eta r} \tag{3.2}$$

This is, however, only appropriate for dilute dispersions where particle diffusion is not influenced by the solvodynamics and presence of other particles. In a DLS measurement, the diffusion coefficient (D) obtained from the decay rate of the first-order autocorrelation function. This is used to infer the solvodynamic radius assuming free motion, but for concentrated dispersions, the diffusion coefficient is decoupled from the radius and is known to decrease as many-body effects begin to influence the particle motion [4].

The dispersions are highly transparent, which means that the more complex light scattering instrumentation required to study concentrated, turbid dispersions [84,85] is not required. We have performed an exploratory measurement of the particle diffusion using commercial DLS instrumentation that measures at fixed Q to obtain reliable data. The diffusion constant is, in fact, calculated from a Q-dependent function of the temporal autocorrelation function measured by the instrument. The product Qr is typically used to compare measurements of different particles and on different instruments. The value of Qr (using r_Z, the Z-average radius from a DLS measurement on a dilute dispersion, for the radius) for $PSMA_{34}$–$PTFEMA_{568}$ nanoparticles and these DLS measurements is 1.6. This is less than for typical measurements on PMMA latexes and is below the structure factor peak; for angle-selective DLS, large Qr are generally targeted [4,86–88]. As we are not in the Q limit where structural contributions or collective motion [5,89,90] can be completely ignored, we refer to the diffusion coefficient as $D(Q)$. These measurements are valuable because they can be obtained with simple instrumentation, but to explore the Q-dependent diffusion of spheres [91], further experiments using more advanced forms of photon correlation spectroscopy, such as XPCS [92,93] would be worth exploring.

A plot of the experimentally obtained diffusion coefficient ($D(Q)$) normalised by the diffusion coefficient of the most dilute dispersion studied ($D_0(Q)$) is shown in Figure 5. As expected, the diffusion coefficient decreases as the particle concentration is increased. The data are compared to the virial expansion of the short-time diffusion coefficient given by Batchelor ($D(Q)/D_0(Q) = 1 - 1.83\phi + 0.88\phi^2$) [94] and agree reasonably well up to a volume fraction of ~ 0.3. This onset of slow dynamics is typically described using the Vogel–Fulcher–Tamman (VFT) form, which can be used to describe the increase in viscosity shown by glass-forming liquids as they are supercooled, or the increase in alpha relaxation (structural relaxation) time with the density of hard sphere suspensions [95] and can be similarly applied to particle diffusion [96], as done in this study. The VFT equation takes the form:

$$D^{-1}(\phi) = D_0^{-1}\frac{A}{(\phi_0 - \phi)} \tag{3.3}$$

where A is a measure of the "fragility" of the system (the degree to which the system slows down as it approaches the glass transition ϕ_g) and ϕ_0 is the volume fraction of a predicted dynamical divergence, which serves as a lower bound for the experimental glass transition ϕ_g.

Figure 5 shows the relationship between effective volume fraction ϕ_{eff} and the diffusion coefficient $D(Q)$. The volume fractions determined from the mass are adjusted by a small constant prefactor to give ϕ_{eff} ($\phi_{\text{eff}} = 0.97\phi$), which are the concentrations that best agree with VFT theory. This behaviour is in very good agreement with VFT-like scaling and predicts a ϕ_0 of 0.619 ± 0.010, in excellent agreement with previously reported values obtained from confocal microscopy and light scattering measurements of the alpha relaxation time (τ_α) of density and refractive index matched PMMA hard spheres [90,97]. The inverse diffusion coefficient and alpha relaxation time are known to diverge at higher densities as self-diffusion and structural relaxation timescales decouple, but over the range of volume fractions covered here this is not expected to be the case [98]. This is reflected in the compatibility of this measurement of ϕ_0 with previous reports. While this agreement is gratifying, there are reasons that this cannot on its own be used to definitely prove hard sphere interactions. As discussed above, we are not in the appropriate Q-limit where structural contributions can be completely ignored, therefore the volume fraction rescaling could be accounting for the presence of interparticle interactions. Nevertheless, that

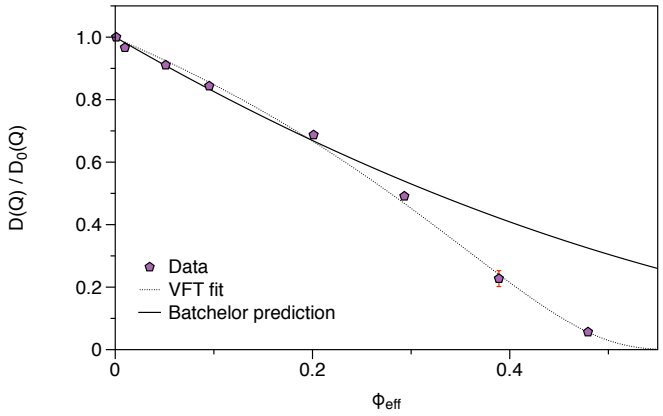

Figure 5. Normalised diffusion coefficient ($D(Q)/D_0(Q)$) as a function of effective volume fraction ($\phi_{\rm eff}$). The diffusion of the particles clearly slows as the dispersions are concentrated, as expected. The solid line is the virial expansion of the short-time diffusion coefficient given by Batchelor [94], which shows reasonable agreement up to $phi_{\rm eff} \approx 0.3$. At greater concentrations, VFT scaling shows good agreement with the data using realistic input parameters.

the diffusion coefficient varies smoothly and predictably over a wide range of volume fractions demonstrates that these particles are stable and do not appear to aggregate at high concentrations, essential for their use as a model system. Further experiments to elucidate the precise degree of interparticle interaction between these particles is warranted and welcome.

4. Conclusions

Due to the popularity and utility of refractive index matched colloids over recent decades, we sought to develop a system of transparent nano-objects consisting of a *single* core-forming polymer in a *single* solvent. This is in contrast to the polymer colloids commonly used, which either require a binary solvent mixture or a binary core-forming polymer. The core-forming polymer of choice was poly(2,2,2-trifluoroethyl methacrylate) (PTFEMA), which being semi-fluorinated has a low polarisability and consequently a relatively low refractive index [99]. As the refractive index difference can be related to the strength of the van der Waals attractions [3], obtaining a transparent dispersion of nanoparticles is a prerequisite to obtaining a non-interacting dispersion.

By synthesising these nano-objects directly in a range of *n*-alkanes, we were able to identify the ideal formulation to obtain transparent dispersions of polymer colloids via PISA: PSMA–PTFEMA in *n*-tetradecane synthesised by PISA using CDB RAFT agent. These particles offer some very appealing properties. Being nearly transparent, light scattering measurements can be performed even at high nanoparticle concentrations, and due to the large electron density difference between polymer and solvent, X-ray scattering measurements can be performed even at concentrations where light scattering measurements are challenging. DLS studies using concentrated dispersions of these PSMA–PTFEMA nano-objects confirmed that it is possible to study such particles at high concentrations. The data show that the particles remain well-dispersed even at high concentrations. However, the size distribution is broader than desirable, which is known to impact the phases that hard spheres form [17,100,101]. For example, colloidal spheres with a size distribution of $\sim 7\%$ will fail to crystallise [17]. In the future, optimising the synthesis conditions will most likely reduce the size distribution by eliminating the minor population of non-spherical nanoparticles. Such refined particles should serve as a useful model system to both explore existing theories of colloidal interactions and inspire new theoretical developments.

Since the first report of colloidal crystals of refractive matched PMMA latexes [2], many subsequent papers have revealed interesting colloid science using these hard sphere colloids [17]. This new system of refractive index matched PSMA–PTFEMA nanoparticles in *n*-tetradecane should enable similarly interesting colloid science experiments in the future. By synthesising these particles using RAFT-mediated PISA, it has been possible to controllably target colloids of a small size (diameters less than ~ 100 nm). In contrast, polymer latexes synthesised in non-polar solvents tend to be well defined only for large particles (diameters up to several μm) [35]. The small diameter of these diblock copolymer nanoparticles does mean that the width of the size distribution (~ 10–15%) is necessarily broader than for typical PMMA latexes (~ 5–6% [17]). However, this small size does provide some advantages and opportunities. Large particles require density matching solvent to prevent significant sedimentation during the course of the experiment, and the solvents used to do this soften the interaction potential [1]. Due to the relatively small size of these particles, their sedimentation velocity is low, even though the density difference between solvent and particle is large. Using Stokes's Law [102], we estimate that these particles would sediment ~ 0.1 mm in a day, much less than the $\lesssim 1$ mm per day threshold proposed by Royall *et al*. [1] and less than ~ 0.1–0.3 mm per day threshold determined to be acceptable for scattering measurements by Washington *et al*. [103]. Additionally, these new particles provide the opportunity of extending studies over a wide range of sizes, due to the versatility of PISA syntheses. This will not only aid in universalising colloidal interactions over a broader length scale, but it will also make possible studies of faster diffusing particles as well. We believe that this system of new refractive index matched PSMA–PTFEMA polymer micelles in *n*-tetradecane offers a useful model experimental model system for studying non-interacting colloids.

Data Accessibility. Particle characterisation details and X-ray scattering fitting values provided in Supporting Information.
Additional research data available from the Zenodo repository (doi:10.5281/zenodo.1475878).

Authors' Contributions. GN Smith devised the experiments, prepared the materials, and performed most experiments. MJ Derry, T Neal, and OO Mykhaylyk supported the SAXS measurements. S Prévost supported SAXS measurements as beamline scientist at the ESRF. JE Hallett performed analysis of the diffusion data. JR Lovett performed TEM measurements. SP Armes supported planning experiments and interpreting data as group leader. All authors read and inputted to the manuscript.

Competing Interests. The authors declare no competing interests.

Funding. ERC (PISA 320372). EPSRC (EP/J007846). STFC (funding for travel to ESRF).

Acknowledgements. The authors acknowledge the ESRF for awarding beamtime on ID02. EJ Cornel and MJ Rymaruk (University of Sheffield, UK) are acknowledged for enlightening discussions.

Address details.
* Current address: Niels Bohr Institute, University of Copenhagen, Universitetsparken 5, 2100 Copenhagen Ø, Denmark
† Current address: Physical & Theoretical Chemistry Laboratory, University of Oxford, South Parks Road, Oxford, OX1 3QZ, UK
‡ Current address: Institut Laue–Langevin, BP 156-X, F-38042 Grenoble Cedex, France

References

1. Royall CP, Poon WCK, Weeks ER. 2013 In search of colloidal hard spheres. Soft Matter **9**, 17–27.
2. Pusey PN, van Megen W. 1986 Phase behaviour of concentrated suspensions of nearly hard colloidal spheres. Nature **320**, 340–342.
3. Israelachvili JN. 1972 The Calculation of Van Der Waals Dispersion Forces between Macroscopic Bodies. Proc. R. Soc. London A: Math., Phys. Eng. Sci. **331**, 39–55.
4. Segrè PN, Behrend OP, Pusey PN. 1995 Short-time Brownian motion in colloidal suspensions: Experiment and simulation. Phys. Rev. E **52**, 5070–5083.

5. Segrè PN, Pusey PN. 1996 Scaling of the Dynamic Scattering Function of Concentrated Colloidal Suspensions. Phys. Rev. Lett. **77**, 771–774.
6. Ueda M, Kim HB, Ichimura K. 1994 Photocontrolled aggregation of colloidal silica. J. Mater. Chem. **4**, 883–889.
7. Senff H, Richtering W. 1999 Temperature sensitive microgel suspensions: Colloidal phase behavior and rheology of soft spheres. J. Chem. Phys. **111**, 1705–1711.
8. Hellweg T, Dewhurst CD, Brückner E, Kratz K, Eimer W. 2000 Colloidal crystals made of poly(*N*-isopropylacrylamide) microgel particles. Colloid Polym. Sci. **278**, 972–978.
9. Wu J, Zhou B, Hu Z. 2003 Phase Behavior of Thermally Responsive Microgel Colloids. Phys. Rev. Lett. **90**, 048304.
10. Underwood SM, Taylor JR, van Megen W. 1994 Sterically Stabilized Colloidal Particles as Model Hard Spheres. Langmuir **10**, 3550–3554.
11. Gasser U, Weeks ER, Schofield A, Pusey PN, Weitz DA. 2001 Real-Space Imaging of Nucleation and Growth in Colloidal Crystallization. Science **292**, 258–262.
12. Royall CP, Leunissen ME, van Blaaderen A. 2003 A new colloidal model system to study long-range interactions quantitatively in real space. J. Phys.: Condens. Matter **15**, S3581–S3596.
13. Royall CP, Leunissen ME, Hynninen AP, Dijkstra M, van Blaaderen A. 2006 Re-entrant melting and freezing in a model system of charged colloids. J. Chem. Phys. **124**, 244706.
14. Kaufman LJ, Weitz DA. 2006 Direct imaging of repulsive and attractive colloidal glasses. J. Chem. Phys. **125**, 074716.
15. Leunissen ME. 2007 Manipulating Colloids with Charges & Electric Fields. PhD thesis Universiteit Utrecht.
16. Ohtsuka T, Royall CP, Tanaka H. 2008 Local structure and dynamics in colloidal fluids and gels. Europhys. Lett. **84**, 46002.
17. Poon WCK, Weeks ER, Royall CP. 2012 On measuring colloidal volume fractions. Soft Matter **8**, 21–30.
18. Underwood SM, van Megen W. 1996 Refractive index variation in nonaqueous sterically stabilized copolymer particles. Colloid Polym. Sci. **274**, 1072–1080.
19. van Megen W, Underwood SM, Müller J, Mortensen TC, Enderson SI, Harland JL, Francis P. 1997 Particle Diffusion and Crystallisation in Suspensions of Hard Spheres. Prog. Theor. Phys. Suppl. **126**, 171–180.
20. Henderson SI, van Megen W. 1998 Metastability and Crystallization in Suspensions of Mixtures of Hard Spheres. Phys. Rev. Lett. **80**, 877–880.
21. Bryant G, Mortensen T, Henderson S, Williams S, van Megen W. 1999 Optical Contrast Variation Study of Nonaqueous Suspensions of Polymer Particles. J. Colloid Interface Sci. **216**, 401–408.
22. Williams SR, van Megen W. 2001 Motions in binary mixtures of hard colloidal spheres: Melting of the glass. Phys. Rev. E **64**, 041502.
23. Bryant G, Martin S, Budi A, van Megen W. 2003 Accurate Measurement of Small Polydispersities in Colloidal Suspensions. Langmuir **19**, 616–621.
24. Martin S, Bryant G, van Megen W. 2003 Crystallization kinetics of polydisperse colloidal hard spheres: Experimental evidence for local fractionation. Phys. Rev. E **67**, 061405.
25. Martin S, Bryant G, van Megen W. 2005 Crystallization kinetics of polydisperse colloidal hard spheres. II. Binary mixtures. Phys. Rev. E **71**, 021404.
26. Martinez VA, Bryant G, van Megen W. 2008 Slow Dynamics and Aging of a Colloidal Hard Sphere Glass. Phys. Rev. Lett. **101**, 135702.
27. van Megen W, Martinez VA, Bryant G. 2009a Scaling of the Space-Time Correlation Function of Particle Currents in a Suspension of Hard-Sphere-Like Particles: Exposing When the Motion of Particles is Brownian. Phys. Rev. Lett. **103**, 258302.
28. van Megen W, Martinez VA, Bryant G. 2009b Arrest of Flow and Emergence of Activated Processes at the Glass Transition of a Suspension of Particles with Hard Spherelike Interactions. Phys. Rev. Lett. **102**, 168301.
29. Martinez VA, Bryant G, van Megen W. 2010 Aging dynamics of colloidal hard sphere glasses. J. Chem. Phys. **133**, 114906.
30. Martinez VA, Thijssen JHJ, Zontone F, van Megen W, Bryant G. 2011 Dynamics of hard sphere suspensions using dynamic light scattering and X-ray photon correlation spectroscopy: Dynamics and scaling of the intermediate scattering function. J. Chem. Phys. **134**, 054505.
31. Kodger TE, Guerra RE, Sprakel J. 2015 Precise colloids with tunable interactions for confocal microscopy. Scientific Reports **5**, 14635.

32. Ottewill RH, Livsey I. 1987 The imbibition of carbon disulphide by poly(methyl methacrylate) latex particles. Polymer **28**, 109 – 113.
33. Smith GN, Finlayson SD, Rogers SE, Bartlett P, Eastoe J. 2017 Electrolyte-induced Instability of Colloidal Dispersions in Nonpolar Solvents. J. Phys. Chem. Lett. **8**, 4668–4672.
34. Stöber W, Fink A, Bohn E. 1968 Controlled growth of monodisperse silica spheres in the micron size range. J. Colloid Interface Sci. **26**, 62–69.
35. Antl L, Goodwin JW, Hill RD, Ottewill RH, Owens SM, Papworth S, Waters JA. 1986 The preparation of poly(methyl methacrylate) latices in non-aqueous media. Colloids Surf. **17**, 67–78.
36. Tseng CM, Lu YY, El-Aasser MS, Vanderhoff JW. 1986 Uniform polymer particles by dispersion polymerization in alcohol. J. Polym. Sci. A: Polym. Chem. **24**, 2995–3007.
37. Maranzano BJ, Wagner NJ, Fritz G, Glatter O. 2000 Surface Charge of 3-(Trimethoxysilyl) Propyl Methacrylate (TPM) Coated Stöber Silica Colloids by Zeta-Phase Analysis Light Scattering and Small Angle Neutron Scattering. Langmuir **16**, 10556–10558.
38. Bosma G, Pathmamanoharan C, de Hoog EH, Kegel WK, van Blaaderen A, Lekkerkerker HN. 2002 Preparation of Monodisperse, Fluorescent PMMA–Latex Colloids by Dispersion Polymerization. J. Colloid Interface Sci. **245**, 292–300.
39. Sánchez R, Bartlett P. 2011 Synthesis of charged particles in an ultra-low dielectric solvent. Soft Matter **7**, 887–890.
40. Canning SL, Smith GN, Armes SP. 2016 A Critical Appraisal of RAFT-Mediated Polymerization-Induced Self-Assembly. Macromolecules **49**, 1985–2001.
41. Derry MJ, Fielding LA, Armes SP. 2015 Industrially-relevant polymerization-induced self-assembly formulations in non-polar solvents: RAFT dispersion polymerization of benzyl methacrylate. Polym. Chem. **6**, 3054–3062.
42. Ratcliffe LPD, McKenzie BE, Bouëdec GMDL, Williams CN, Brown SL, Armes SP. 2015 Polymerization-Induced Self-Assembly of All-Acrylic Diblock Copolymers via RAFT Dispersion Polymerization in Alkanes. Macromolecules **48**, 8594–8607.
43. Warren NJ, Armes SP. 2014 Polymerization-Induced Self-Assembly of Block Copolymer Nano-objects via RAFT Aqueous Dispersion Polymerization. J. Am. Chem. Soc. **136**, 10174–10185.
44. Derry MJ, Fielding LA, Armes SP. 2016 Polymerization-induced self-assembly of block copolymer nanoparticles via RAFT non-aqueous dispersion polymerization. Prog. Polym. Sci. **52**, 1–18.
45. Lowe AB. 2016 RAFT alcoholic dispersion polymerization with polymerization-induced self-assembly. Polymer **106**, 161–181.
46. Houillot L, Bui C, Save M, Charleux B, Farcet C, Moire C, Raust JA, Rodriguez I. 2007 Synthesis of Well-Defined Polyacrylate Particle Dispersions in Organic Medium Using Simultaneous RAFT Polymerization and Self-Assembly of Block Copolymers. A Strong Influence of the Selected Thiocarbonylthio Chain Transfer Agent. Macromolecules **40**, 6500–6509.
47. Houillot L, Bui C, Farcet C, Moire C, Raust JA, Pasch H, Save M, Charleux B. 2010 Dispersion Polymerization of Methyl Acrylate in Nonpolar Solvent Stabilized by Block Copolymers Formed In situ via the RAFT Process. ACS Appl. Mater. Interfaces **2**, 434–442.
48. Raust JA, Houillot L, Save M, Charleux B, Moire C, Farcet C, Pasch H. 2010 Two Dimensional Chromatographic Characterization of Block Copolymers of 2-Ethylhexyl Acrylate and Methyl Acrylate, P2EHA-*b*-PMA, produced via RAFT-Mediated Polymerization in Organic Dispersion. Macromolecules **43**, 8755–8765.
49. Fielding LA, Derry MJ, Ladmiral V, Rosselgong J, Rodrigues AM, Ratcliffe LPD, Sugihara S, Armes SP. 2013 RAFT dispersion polymerization in non-polar solvents: facile production of block copolymer spheres, worms and vesicles in *n*-alkanes. Chem. Sci. **4**, 2081–2087.
50. Fielding LA, Lane JA, Derry MJ, Mykhaylyk OO, Armes SP. 2014 Thermo-responsive Diblock Copolymer Worm Gels in Non-polar Solvents. J. Am. Chem. Soc. **136**, 5790–5798.
51. Lopez-Oliva AP, Warren NJ, Rajkumar A, Mykhaylyk OO, Derry MJ, Doncom KEB, Rymaruk MJ, Armes SP. 2015 Polydimethylsiloxane-Based Diblock Copolymer Nano-objects Prepared in Nonpolar Media via RAFT-Mediated Polymerization-Induced Self-Assembly. Macromolecules **48**, 3547–3555.
52. Derry MJ, Fielding LA, Warren NJ, Mable CJ, Smith AJ, Mykhaylyk OO, Armes SP. 2016 *In situ* small-angle X-ray scattering studies of sterically-stabilized diblock copolymer nanoparticles

formed during polymerization-induced self-assembly in non-polar media. Chem. Sci. **7**, 5078–5090.
53. Derry MJ, Mykhaylyk OO, Armes SP. 2017 A Vesicle-to-Worm Transition Provides a New High-Temperature Oil Thickening Mechanism. Angew. Chem. Int. Ed. **56**, 1746–1750.
54. Maiti B, Bauri K, Nandi M, De P. 2017 Surface functionalized nano-objects from oleic acid-derived stabilizer via non-polar RAFT dispersion polymerization. J. Polym. Sci. A: Polym. Chem. **55**, 263–273.
55. Smith GN, Mears LLE, Rogers SE, Armes SP. 2018 Synthesis and electrokinetics of cationic spherical nanoparticles in salt-free non-polar media. Chem. Sci. **9**, 922–934.
56. Derry MJ, Mykhaylyk OO, Ryan AJ, Armes SP. 2018 Thermoreversible crystallization-driven aggregation of diblock copolymer nanoparticles in mineral oil. Chem. Sci. **9**, 4071–4082.
57. Pei Y, Thurairajah L, Sugita OR, Lowe AB. 2015a RAFT Dispersion Polymerization in Nonpolar Media: Polymerization of 3-Phenylpropyl Methacrylate in n-Tetradecane with Poly(stearyl methacrylate) Homopolymers as Macro Chain Transfer Agents. Macromolecules **48**, 236–244.
58. Pei Y, Noy JM, Roth PJ, Lowe AB. 2015b Soft Matter Nanoparticles with Reactive Coronal Pentafluorophenyl Methacrylate Residues via Non-Polar RAFT Dispersion Polymerization and Polymerization-Induced Self-Assembly. J. Polym. Sci. A: Polym. Chem. **53**, 2326–2335.
59. Pei Y, Sugita OR, Thurairajah L, Lowe AB. 2015c Synthesis of poly(stearyl methacrylate-*b*-3-phenylpropyl methacrylate) nanoparticles in *n*-octane and associated thermoreversible polymorphism. RSC Adv. **5**, 17636–17646.
60. Cunningham VJ, Armes SP, Musa OM. 2016 Synthesis, characterisation and Pickering emulsifier performance of poly(stearyl methacrylate)–poly(*N*-2-(methacryloyloxy)ethyl pyrrolidone) diblock copolymer nano-objects *via* RAFT dispersion polymerisation in *n*-dodecane. Polym. Chem. **7**, 1882–1891.
61. Canning SL, Cunningham VJ, Ratcliffe LPD, Armes SP. 2017 Phenyl acrylate is a versatile monomer for the synthesis of acrylic diblock copolymer nano-objects via polymerization-induced self-assembly. Polym. Chem. **8**, 4811–4821.
62. Cornel EJ, van Meurs S, Smith T, O'Hora PS, Armes SP. 2018 In Situ Spectroscopic Studies of Highly Transparent Nanoparticle Dispersions Enable Assessment of Trithiocarbonate Chain-End Fidelity during RAFT Dispersion Polymerization in Nonpolar Media. J. Am. Chem. Soc. **140**, 12980–12988.
63. Semsarilar M, Jones ER, Armes SP. 2014 Comparison of pseudo-living character of RAFT polymerizations conducted under homogeneous and heterogeneous conditions. Polym. Chem. **5**, 195–203.
64. Rymaruk MJ, Thompson KL, Derry MJ, Warren NJ, Ratcliffe LPD, Williams CN, Brown SL, Armes SP. 2016 Bespoke contrast-matched diblock copolymer nanoparticles enable the rational design of highly transparent Pickering double emulsions. Nanoscale **8**, 14497–14506.
65. Harrisson S. 2018 The downside of dispersity: why the standard deviation is a better measure of dispersion in precision polymerization. Polym. Chem. **9**, 1366–1370.
66. Ilavsky J. 2012 *Nika*: software for two-dimensional data reduction. J. Appl. Cryst. **45**, 324–328.
67. Boesecke P. 2007 Reduction of two-dimensional small- and wide-angle X-ray scattering data. J. Appl. Cryst. **40**, s423–s427.
68. Ilavsky J, Jemian PR. 2009 *Irena*: tool suite for modeling and analysis of small-angle scattering. J. Appl. Cryst. **42**, 347–353.
69. van de Hulst HC. 1957 Light Scattering by Small Particles. Mineola, NY: Dover Publications.
70. CRC. 2014–2015 (Internet Version) Physical Constants of Organic Compounds. In CRC Handbook of Chemistry and Physics. CRC Press 95th edition.
71. Tamada M, Asano M, Yoshida M, Kumakura M. 1991 Formation of a thin film of poly(octadecyl methacrylate) using the physical vapour deposition technique. Polymer **32**, 2064–2069.
72. Yoshioka H, Itoh Y, Kiyomori A, Era M, Oki Y. 2013 Fluorene-based chromophore for degradation-recoverable solid-state dye laser. Opt. Mater. Express **3**, 176–183.
73. Nakagaki M, Heller W. 1956 Effect of Light Scattering upon the Refractive Index of Dispersed Colloidal Spheres. J. Appl. Phys. **27**, 975–979.
74. Grillo I. 2008 pp. 723–782. In Small-Angle Neutron Scattering and Applications in Soft Condensed Matter, pp. 723–782. Dordrecht: Springer Netherlands.
75. Blanazs A, Madsen J, Battaglia G, Ryan AJ, Armes SP. 2011 Mechanistic Insights for Block Copolymer Morphologies: How Do Worms Form Vesicles?. J. Am. Chem. Soc. **133**, 16581–16587.

76. Pedersen JS, Gerstenberg MC. 1996 Scattering Form Factor of Block Copolymer Micelles. Macromolecules **29**, 1363–1365.
77. Pedersen JS, Schurtenberger P. 1996 Scattering Functions of Semiflexible Polymers with and without Excluded Volume Effects. Macromolecules **29**, 7602–7612.
78. Pedersen JS. 2000 Form factors of block copolymer micelles with spherical, ellipsoidal and cylindrical cores. J. Appl. Cryst. **33**, 637–640.
79. Pedersen JS, Svaneborg C, Almdal K, Hamley IW, Young RN. 2003 A Small-Angle Neutron and X-ray Contrast Variation Scattering Study of the Structure of Block Copolymer Micelles: Corona Shape and Excluded Volume Interactions. Macromolecules **36**, 416–433.
80. Pedersen JS, Gerstenberg MC. 2003 The structure of P85 Pluronic block copolymer micelles determined by small-angle neutron scattering. Colloids Surf. A: Physicochem. Eng. Aspects **213**, 175–187.
81. Perrier S. 2017 *50th Anniversary Perspective*: RAFT Polymerization—A User Guide. Macromolecules **50**, 7433–7447.
82. Einstein A. 1906 Eine neue Bestimmung der Moleküldimensionen. Ann. Phys. **324**, 289–306.
83. Einstein A. 1911 Berichtigung zu meiner Arbeit: „Eine neue Bestimmung der Moleküldimensione". Ann. Phys. **339**, 591–592.
84. Rojas LF, Vavrin R, Urban C, Kohlbrecher J, Stradner A, Scheffold F, Schurtenberger P. 2003 Particle dynamics in concentrated colloidal suspensions. Faraday Discuss. **123**, 385–400.
85. Rojas-Ochoa LF, Castañeda Priego R, Lobaskin V, Stradner A, Scheffold F, Schurtenberger P. 2008 Density Dependent Interactions and Structure of Charged Colloidal Dispersions in the Weak Screening Regime. Phys. Rev. Lett. **100**, 178304.
86. van Megen W, Underwood SM, Pusey PN. 1991 Nonergodicity parameters of colloidal glasses. Phys. Rev. Lett. **67**, 1586–1589.
87. van Megen W, Underwood SM. 1993a Dynamic-light-scattering study of glasses of hard colloidal spheres. Phys. Rev. E **47**, 248–261.
88. van Megen W, Underwood SM. 1993b Glass transition in colloidal hard spheres: Mode-coupling theory analysis. Phys. Rev. Lett. **70**, 2766–2769.
89. Segrè PN, Pusey PN. 1997 Dynamics and scaling in hard-sphere colloidal suspensions. Physica A: Stat. Mech. Appl. **235**, 9–18.
90. Brambilla G, El Masri D, Pierno M, Berthier L, Cipelletti L, Petekidis G, Schofield AB. 2009 Probing the equilibrium dynamics of colloidal hard spheres above the mode-coupling glass transition. Phys. Rev. Lett. **102**, 085703.
91. Beenakker CWJ, Mazur P. 1984 Diffusion of spheres in a concentrated suspension II. Physica A: Stat. Mech. Appl. **126**, 349–370.
92. Grübel G, Madsen A, Robert A. 2008 pp. 953–995. In X-Ray Photon Correlation Spectroscopy (XPCS), pp. 953–995. Dordrecht: Springer Netherlands.
93. Leheny RL. 2012 XPCS: Nanoscale motion and rheology. Curr. Opin. Colloid Interface Sci. **17**, 3–12.
94. Batchelor GK. 1976 Brownian diffusion of particles with hydrodynamic interaction. J. Fluid Mech. **74**, 1–29.
95. Royall CP, Williams SR. 2015 The role of local structure in dynamical arrest. Physics Reports **560**, 1–75.
96. Sastry S. 2000 Liquid limits: Glass transition and liquid-gas spinodal boundaries of metastable liquids. Phys. Rev. Lett. **85**, 590.
97. Pinchaipat R, Campo M, Turci F, Hallett JE, Speck T, Royall CP. 2017 Experimental evidence for a structural-dynamical transition in trajectory space. Phys. Rev. Lett. **119**, 028004.
98. Weysser F, Puertas AM, Fuchs M, Voigtmann T. 2010 Structural relaxation of polydisperse hard spheres: Comparison of the mode-coupling theory to a Langevin dynamics simulation. Phys. Rev. E **82**, 011504.
99. Groh W, Zimmermann A. 1991 What is the lowest refractive index of an organic polymer?. Macromolecules **24**, 6660–6663.
100. Sollich P, Wilding NB. 2011 Polydispersity induced solid-solid transitions in model colloids. Soft Matter **7**, 4472–4484.
101. Fasolo M, Sollich P. 2003 Equilibrium Phase Behavior of Polydisperse Hard Spheres. Phys. Rev. Lett. **91**, 068301.
102. Stokes GG. 1851 On the Effect of the Internal Friction of Fluids on the Motion of Pendulums. Trans. Camb. Phil. Soc. **IX**, 8–18.

103. Washington AL, Li X, Schofield AB, Hong K, Fitzsimmons MR, Dalgliesh R, Pynn R. 2014 Inter-particle correlations in a hard-sphere colloidal suspension with polymer additives investigated by Spin Echo Small Angle Neutron Scattering (SESANS). Soft Matter **10**, 3016–3026.